

## Evaluation of Cleome Droserifolia (Samwah) as Green Corrosion Inhibitor for Mild Steel in 1 M HCl Solution

Abd El-Aziz S. Fouda<sup>1</sup>, Rabab M. Abou Shahba<sup>2</sup>, Azza E. El-Shenawy<sup>2</sup>, Taghreed J.A. Seyam<sup>3</sup>

<sup>1</sup> Department of Chemistry, Faculty of Science, El-Mansoura University, El-Mansoura-35516, Egypt

<sup>2</sup> Department of Chemistry, Faculty of Science (Girls branch), Al-Azhar University, Cairo, Egypt

<sup>3</sup> Ministry of Education and Higher Education, Gaza, Palestine

\*E-mail: [asfouda@hotmail.com](mailto:asfouda@hotmail.com)

Received: 12 August 2017 / Accepted: 6 October 2017 / Published: 5 June 2018

---

Cleome Droserifolia (Samwah) extract (CDE) was investigated for its capability to prevent mild steel (MS) corrosion in HCl (1.0 M) by means of mass loss (ML) and electrochemical (e.g. Tafel polarization (TP), electrochemical frequency modulation (EFM), electrochemical impedance spectroscopy (EIS)) techniques. The inhibitor protection (IP) improved with rise in inhibitor concentration and lowered with decrease the temperature. Tafel polarization (TP) showed that this extract acts as mixed kind inhibitor. CDE was adsorbed physically on MS surface obeying Langmuir adsorption isotherm. Surface analyses via atomic force microscope (AFM) and scanning electron (SEM) showed a significant surface of the MS. The CDE was used to be the best corrosion inhibitor for MS in 1.0 M HCl as all utilized techniques report.

---

**Keywords:** Corrosion inhibition, Cleome Droserifolia (Samwah) extract, mild steel, HCl, SEM, AFM

### 1. INTRODUCTION

Mild steel has been the most widely utilized alloy for structural and manufacturing uses for example: industries mining, construction and metal processing equipment [1]. Acidic solutions have been broadly utilized in washing, oil well acidizing scraping and pickling demanding the utilize of corrosion hinder to lower their attack (corrosion) on metallic materials. Inhibitors inhibit corrosion both by creating a shielding oxide film and by adsorption among aromatic ( $\pi$  electrons) and heteroatoms such as (P, S, O and N) by generating a barrier that inhibits the admittance of destructive agents to the surface of metal [2, 3]. Consequently, research have progressively discovered by utilizing of the non-toxic and ecofriendly inhibitors (Green corrosion inhibitors) for example plant extracts [4, 5]. In modern years, large researches have attentive on the corrosion hindrance concert of extracts from

an environmentally friendly plant to escape the negative effect of man-made corrosion protection [6-8]. CDE leaves and flowers extract, locally known as Samwah, belongs to the Cleomaceae family. It grows in Egypt, Libya, Palestine and Syria as it requires a stony and sandy soil [9].

The aim of the present study is to examine the corrosion hindrance effect of CDE as an inexpensive and environment friendly corrosion protection for MS in 1M HCl medium by (ML), (TP), (EIS) and (EFM) tests. The shielding film made on the surface of metal was examined with the help of FT-IR spectroscopy, SEM and AFM techniques.

## 2. EXPERIMENTAL METHODS

### 2.1. MS specimen composition

The chemical structure of MS specimen in weight % is: (C) 0.068, (Si) 0.022, (S) 0.006, (Mn) 0.169, (Ni) 0.011, (Cr) 0.004, (Mo) 0.005, (Cu) 0.045, (Ti) 0.001, (Co) 0.005, (Al) 0.033 and the rest (Fe).

### 2.2. Preparation of MS specimens

Seven coins of MS of size 2 cm×2 cm x 2 cm with a slight hole of round 2 mm length for ML test. For TP and EIS test, the MS was fused with a platinum cable for electrical linking and was surrounded in epoxy resin to representation a geometrical surface 1 cm<sup>2</sup>. Coins were polished to yield a hand mirror by utilizing emery papers and washed by water and degreased with acetone.

### 2.3 Preparation of test solutions

An appropriate concentration of 37% HCl was prepared in twice distilled water. The concentration range of CDE was wide-ranging from 50 to 300 ppm.

### 2.4. Ready of CDE

The existing search was approved utilized the CDE plant. The samples were obtained from the market and crushed into a fine particle to obtain 200 g and separately soaked in 70% methanol (300 ml) for 48h at room temperature. After that the extract was concentrated to nearly dryness under lower pressure by utilizing the rotating evaporator at 45°C to concentrate the methanol extract [10].

### 2.5 Employed techniques

#### 2.5.1. Mass loss (ML) method (chemical technique)

ML test were achieved on the MS coins in 1M HCl in the presence and absence of various concentrations of CDE. Every single coin was weighed by digital balance and then putted in the acid

medium (100 ml). After the required period, the specimen of MS was washed by twice distilled and weighed again in order to measure the rate of corrosion (CR) and inhibition efficiency (IE %). For each test, a newly solution was prepared to utilize, and the temperature of the solution was controlled by using water thermostat. The ( $\theta$ ) and (IE %) were determined using the following Eq. [11],

$$\% \text{IE} = 100 \times \theta = 100 \times [1 - (\Delta W_{\text{inh}} / \Delta W_{\text{free}})] \quad (1)$$

Where  $\Delta W_{\text{free}}$  and  $\Delta W_{\text{inh}}$  is the MLs of MS in the absence and presence of CDE, correspondingly.

### 2.5.2. Electrochemical techniques

Electrochemical techniques used (TP, EIS, EFM) for the corrosion study was described previously [12]. The tests for research have made by utilizing a Gamry three-electrode cell. The MS of 1 cm<sup>2</sup> act as working electrode (WE), Pt electrode was utilized as an auxiliary, and reference utilized, saturated calomel electrode (SCE). WE scratched with various emery paper. All the tests have achieved for MS coins in 100 ml of 1M HCl in the absence and presence of various concentration of CDE at room temperature. All electrochemical tests were conducted using Gamry Apparatus (PCI4/750). This contains a Gamry framework system based on the ESA 400.

#### 2.5.2.1 Tafel polarization (TP) measurements

The Tafel diagrams were gotten by automatically exchanging the electrode potential from - 0.5 to 0.5 V with an OCP, at a scan rate of 1 mV s<sup>-1</sup>. The linear Tafel sections of the cathodic diagrams and the measured anodic Tafel lines had generalized to the point of connection to give current corrosion density ( $i_{\text{corr}}$ ) and potential ( $E_{\text{corr}}$ ) [13]. Then  $i_{\text{corr}}$  found for measure (IE %) and ( $\theta$ ) as in next:

$$\% \text{IE} = 100 \times \theta = 100 \times [1 - (i_{\text{inh}} / i_{\text{free}})] \quad (2)$$

Where  $i_{\text{free}}$  and  $i_{\text{inh}}$  are the current densities of uninhibited and inhibited solution, respectively.

#### 2.5.2.2 Electrochemical impedance spectroscopy (EIS) measurements

EIS test occurred in a range of frequency (1 Hz to 100 kHz). The data of charge transfer resistance ( $R_{\text{ct}}$ ) obtained from the semicircles diameter of the Nyquist diagrams. The results obtained are from Nyquist and Bode diagrams. The IE% of the inhibitor and ( $\theta$ ) measured by the following:

$$\% \text{IE} = \theta \times 100 = [1 - (R_{\text{ct}}^{\circ} / R_{\text{ct}})] \times 100 \quad (3)$$

Where  $R_{\text{ct}}^{\circ}$  and  $R_{\text{ct}}$  are the charge transfer resistances in the absence and presence of CDE inhibitor, correspondingly.

#### 2.5.2.3. Electrochemical frequency modulation (EFM) measurements

EFM, was accepted by utilized 2 and 5 Hz frequencies. The greater peaks had utilized to measure ( $i_{\text{corr}}$ ), (CF-2& CF-3) causality factors and the ( $\beta_{\text{a}}$  and  $\beta_{\text{c}}$ ) Tafel slopes [14].

## 2.6. Fourier transforms infrared spectroscopy (FT-IR) test

The coins MS were accumulated in 100 ml of 1M HCl in the absence and presence of 300 ppm of CDE inhibitor at room temperature. After 4 h, the coins were removed and dried by air. Then, the MS surface coating on the coins has carefully scratched and the golden coins utilized to the FT-IR spectrum test. IR Affinity (Perkin-Elmer) spectrophotometer was used for recording the FT-IR spectra to define the composition of the corrosion product obtained on the surface of MS.

## 2.7 Surface morphology

### 2.7.1 Scanning electron microscope (SEM) test

Apparatus (JEOL JSM-5500, JAPAN) utilized for reading the picture of the MS coins visible to aggressive solutions in the presence and absence of the CDE extract. MS coins of area  $2 \times 2 \times 2 \text{ cm}^3$  were visible to 100 ml of the destructive solution (1M HCl) for 24h at room temperature, then coins of MS have detached and dried using utilized air.

### 2.7.2 AFM analysis

The coins utilized for external morphology check were immersed in 1M (HCl) for 24 h in the absence and presence of CDE at room temperature then removed from the test solution. The test achieved by the AFM technique was utilized on a Pico SPM2100. AFM expedient working in contact mode in air at Nanotechnology Laboratory, Faculty of Engineering Mansoura University

## 3. RESULTS AND DISCUSSION

### 3.1 Mass loss (ML) measurements

The ML examination of the rate of corrosion and IE is valuable due to its modest application and great constancy [15]. ML tests have done for MS in the absence and presence of various concentrations of CDE ranging from 50 to 300 ppm are shown in Figure (1). The corrosion parameters such as CR, IE %, and  $\theta$  were measured by eq. (1) and recorded in Table (1). The results clearly show that the IE % improves with the rise of concentration reach the higher value of IE% at a maximum concentration (300 ppm). This recommends that rise in the CDE concentration improves the adsorbed molecules above the surface of MS, blocking the active center that attacked by acid and hence, decrease the attack of MS. The lower in IE with the rise of the temperature is characterized by the adsorption physical [16]. In addition, the corrosion rate improved with temperature rise. Due to increased temperatures, the MS corrosion, increased due to the desorption of CDE components partly from the MS surface [17]. Also from the data, it observed that lowering of CR related with rise in the

CDE concentration and lower temperature in which indicates CDE components adsorbed on the MS or at the solution interface on improving its concentration and providing wider surface coverage.

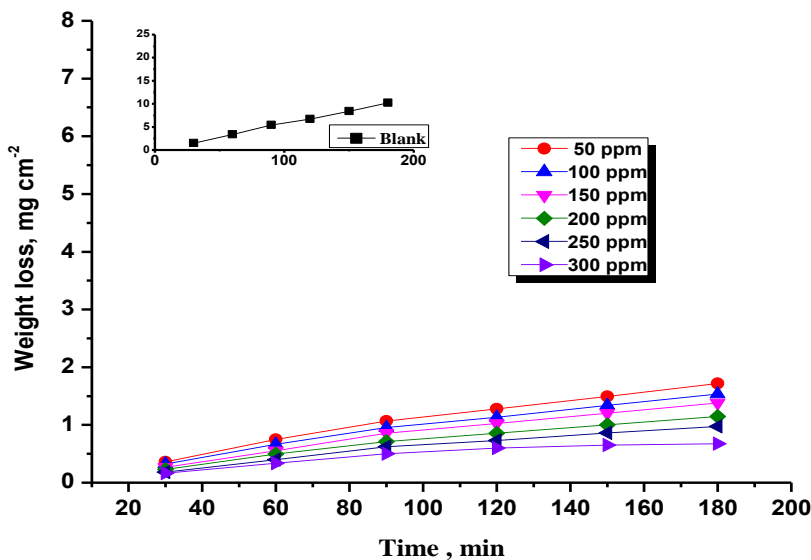


**Figure 1.** Mass loss- time diagrams for the MS corrosion in the absence and presence of various concentrations of CDE at 25°C

**Table 1.** Results of ML tests for MS in the absence and presence of various concentrations of CDE at 25–45°C

Conc., ppm	Temp., °C	C.R.,(mg cm <sup>-2</sup> min <sup>-1</sup> )	θ	%IE
50	25	0.0106	0.811	81.1
	30	0.0155	0.790	79.0
	35	0.025	0.772	77.2
	40	0.039	0.722	72.2
	45	0.053	0.676	67.6
100	25	0.0094	0.832	83.2
	30	0.0140	0.811	81.1
	35	0.0231	0.789	78.9
	40	0.0370	0.740	74.0
	45	0.048	0.703	70.3
150	25	0.0085	0.848	84.8
	30	0.0126	0.830	83.0
	35	0.0205	0.813	81.3
	40	0.0336	0.764	76.4
	45	0.0451	0.725	72.5
200	25	0.0071	0.873	87.3
	30	0.0111	0.849	84.9
	35	0.0185	0.831	83.1
	40	0.0296	0.792	79.2
	45	0.0405	0.753	75.3
	25	0.0060	0.892	89.2

250	30	0.0094	0.872	87.2
	35	0.0162	0.852	85.2
	40	0.0263	0.815	81.5
	45	0.0356	0.783	78.3
300	25	0.0049	0.911	91.1
	30	0.0081	0.890	89.0
	35	0.0139	0.873	87.3
	40	0.0232	0.837	83.7
	45	0.0298	0.818	81.8

3.2 Analysis of TP study

The results obtained from Tafel plots such as  $E_{corr}$ ,  $i_{corr}$ , ( $\beta_a$ ,  $\beta_c$ ) and IE% are recorded in Table (2). The values of  $E_{corr}$  did not change in a regular way from the blank data. This indicates that the CDE acts via mixed protection mode. It is noticeable from Fig (3) that Tafel diagrams had moved decidedly too minimum  $i_{corr}$  as the CDE concentration is improved. The data of  $i_{corr}$  are lowered gradually from blank data ( $1250 \mu A cm^{-2}$ ) to improve in CDE concentration from 50 to 300 ppm. This lower in  $i_{corr}$  is a sign of improving in IE% from 82.6% to 92.6%. The data of  $\beta_a$  and  $\beta_c$  exchange upon adding of CDE from the aggressive acid, which indicates that the extract is a mixed kind inhibitor [18, 19].

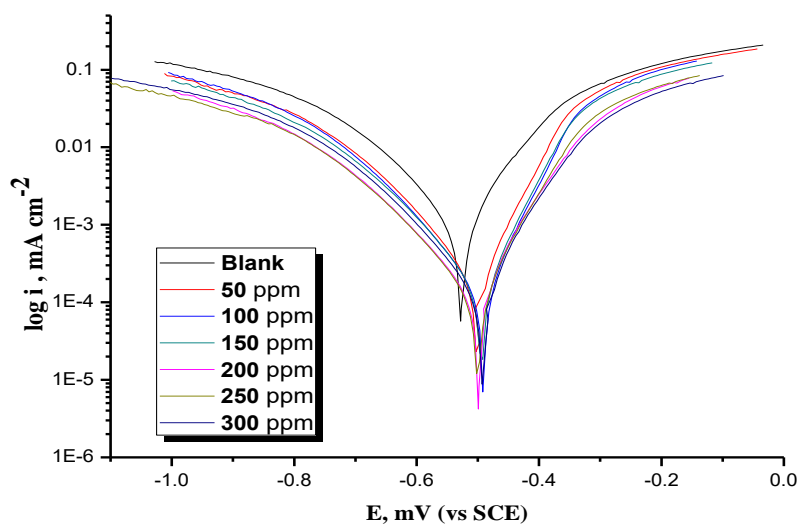


Figure 3. TP diagrams for the MS corrosion of in 1M HCl in the absence and presence of various concentrations of CDE at 25°C

Table 2. Results data of MS in hydrochloric acid in the absence and presence of various concentrations of CDE obtained from TP method at 25°C

[inh.] ppm	- $E_{corr}$ , mV vs SCE	$i_{corr}$ , $\mu A cm^{-2}$	$\beta_c$ , mV dec <sup>-1</sup>	$\beta_a$ , mV dec <sup>-1</sup>	C.R, Mpy	$\theta$	% IE
0	528	1250	132	94	445	--	--

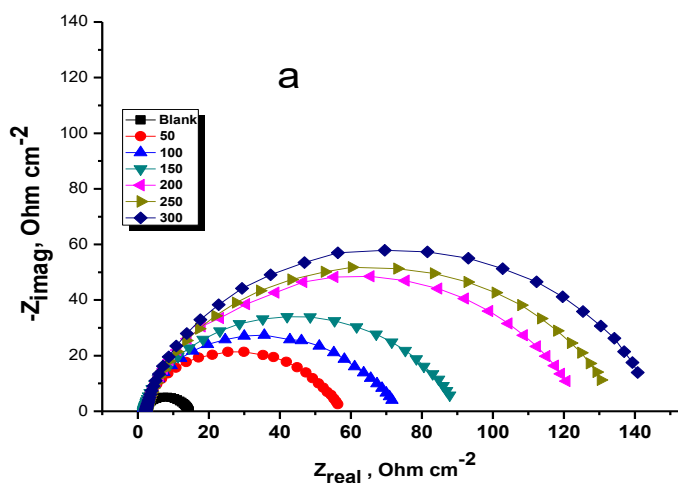
50	510	217	122	73	98	0.826	82.6
100	515	158	116	70	75	0.874	87.4
150	520	151	120	68	70	0.879	87.9
200	490	112	118	76	65	0.910	91.0
250	495	101	124	79	58	0.919	91.9
300	500	92	128	71	55	0.926	92.6

### 3.3 Analysis of EIS study

EIS display a single semicircle agreeing to one time constant in the Bode diagrams (Fig.4b) and the diameter of the semicircle improves with a rise in CDE concentration (Fig 4a), in the impedance of double film and in the higher phase angle (Fig.4 b) In all samples, the Nyquist diagrams were not excellent semicircles. These obtained values can be qualified to the roughness and the inhomogeneity of the electrode of MS [20]. Based on the outline of Nyquist diagrams, the equivalent simplest circuit Figure (5) utilized for appropriate of the EIS data. In this equivalent circuit, resistance of the solution ( $R_s$ ) was in sequence with resistance charge transfer ( $R_{ct}$ ) and ( $C_{dl}$ ). The data of  $R_{ct}$  measured from the various in EIS at the minimum and maximum frequencies [21]. The  $C_{dl}$  can be calculated from the next:

$$C_{dl} = 1 / 2\pi R_{ct} f_{max} \tag{4}$$

Where  $f_{max}$  = the maximum frequency at which imaginary data arrived to a higher on the Nyquist diagrams. Various parameters obtained from impedance  $C_{dl}$ ,  $R_{ct}$  and IE % are recorded in Table (3). The increase in  $R_{ct}$  values with increasing CDE concentrations because the creation of barrier layer on the interfaces of metal/solution [22]. This recommends that the inhibition by CDE qualified to the inhibitor adsorbed of on the MS [23]. The breakdown in  $C_{dl}$  can result from a lower in local dielectric constant and/or improve in the wideness of the electric double layer. All the overhead results conclude to improve in CDE concentration, the protective layer is more and more inhibition. It is clear that there is an excellent agreement among the two various electrochemical tests, due to they gave the same trend of inhibition of CDE



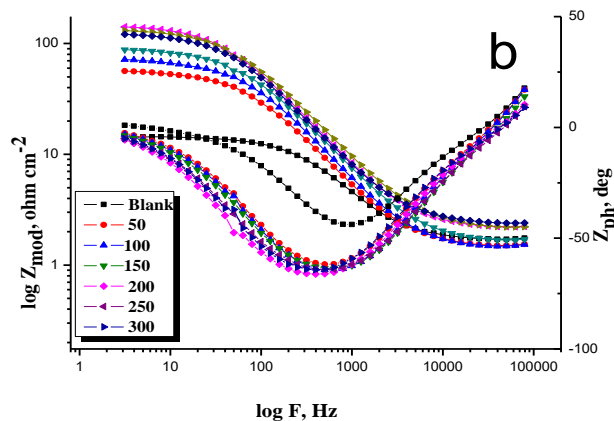


Figure 4 Nyquist (a) and Bode (b) plots of MS in HCl 1M with various concentrations of CDE.

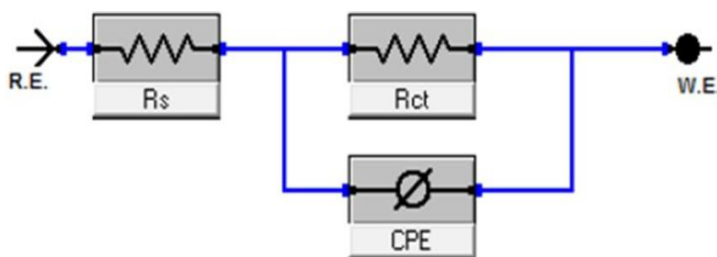


Figure 5. Circuit used to fit EIS values for MS in HCl solutions

Table 3. Parameters obtained from EIS for the MS corrosion in the absence and presence of various concentrations of CDE at 25.0°C

[inh], ppm	$R_{ct}$ , $\Omega \text{ cm}^2$	$C_{dl}$ , $\mu\text{F cm}^{-2}$	$\theta$	% IE
0.0	12.3	47.0	--	--
50	53.4	36.7	0.769	76.9
100	67.9	32.8	0.818	81.8
150	83.7	28.3	0.853	85.3
200	116.0	27.5	0.893	89.3
250	122.1	26.3	0.899	89.9
300	137.5	23.0	0.900	90.0

### 3.4 Analysis of EFM study

EFM Like EIS has a small signal AC technique, but this technique has two sine waves pragmatic to the cell concurrently. EFM is a nondestructive corrosion calculation test that can straight get data on the  $i_{corr}$  deprived of prior information of Tafel constants. Figure 6 shows the EFM spectra (current vs. frequency) without and with various concentrations of CDE for MS corrosion in aggressive medium at 25.0°C. The spectra analyzed to measure  $i_{corr}$ ,  $\beta_a$ ,  $\beta_c$ , CF-2 and CF-3 (causality factors) which itemized in Table (4). It is rich from the obtained value that,  $i_{corr}$  data are lowered by

improving the concentration of CDE, and hence the IE improved. The CFs in Table (4) is very near to their theoretical data conferring to the theory from EFM [24].

**Table 4.** Results data given by EFM test for MS in the absence and presence of various concentrations of CDE at 25.0°C

[inh.] ppm	$i_{corr}$ , $\mu\text{A cm}^{-2}$	$\beta_c$ , $\text{mVdec}^{-1}$	$\beta_a$ , $\text{mVdec}^{-1}$	CF-2	CF-3	C.R, mpy	$\theta$	%IE
Blank	1424	112	94	1.7	2.3	650	--	--
50	273.7	94	83	1.8	2.8	125	0.807	80.7
100	212.1	102	102	1.3	2.8	96	0.851	85.1
150	205.3	93	84	1.8	2.9	91	0.855	85.5
200	142.7	90	83	1.9	3.1	73	0.899	89.9
250	135.9	89	82	2.1	2.9	65	0.905	90.5
300	109.3	80	78	1.8	3.0	51	0.923	92.3

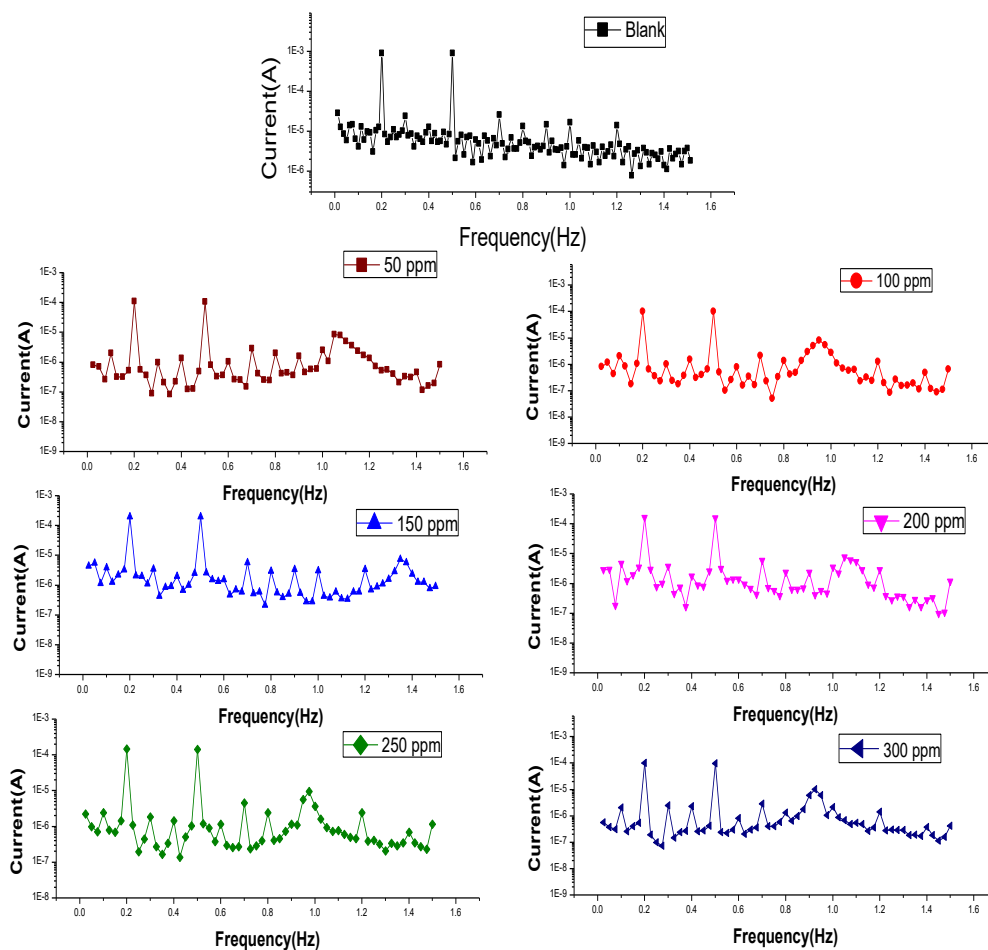


**Figure 6.** EFM data for the MS corrosion with and without various concentrations of CDE at 25.0°C

### 3.5 Adsorption isotherms

Adsorption isotherms are more informative in knowing the nature of relations among inhibitor CDE and the surface of metal substrates [25]. The  $(\theta)$  gotten from ML test was utilized to estimate the greatest isotherm that fits into the gotten values. Isotherm Langmuir was useful to examine whether it finest fits with the results gotten values by utilizing eq. (5) [26].

$$C/\theta = 1/ K_{ads} + C \tag{5}$$

Where C is CDE concentration and  $K_{ads}$  is adsorption equilibrium constant. The diagrams of  $C/\theta$  against C yielded straight lines as shown in Fig. (7), using  $K_{ads}$  values,  $(\Delta G^{\circ}_{ads})$  was measured from the behind eq. (6):

$$\Delta G^{\circ}_{ads} = -RT \ln 55.5K_{ads} \tag{6}$$

The results data of 55.5 is the water concentration in the medium in  $\text{mol L}^{-1}$ . To calculate the heat of adsorption  $(\Delta H^{\circ}_{ads})$ , a diagram of  $\log K_{ads}$  vs.  $1/T$  was done (Fig.8), the slope would be equivalent to  $\Delta H^{\circ}_{ads}/R$  according to the following eq. (7):

$$\text{Log } K_{ads} = (-\Delta H^{\circ}_{ads}/2.303RT) + \text{constant} \tag{7}$$

The  $(\Delta S^{\circ}_{ads})$ , can be obtained from the behind:

$$\Delta G^{\circ}_{ads} = \Delta H^{\circ}_{ads} - T \Delta S^{\circ}_{ads} \tag{8}$$

The  $(K_{ads})$  data,  $(\Delta G^{\circ}_{ads})$ , enthalpy of adsorption  $(\Delta H^{\circ}_{ads})$  and  $(\Delta S^{\circ}_{ads})$  are registered in Table 5. It is seen that all free energy values (Table 5) are negative, indicating spontaneous adsorption of the extract on MS surface and a range of free energy values around -20 kJ/mol indicating that the nature of adsorbed extract is physical for CDE in 1M HCl [27].

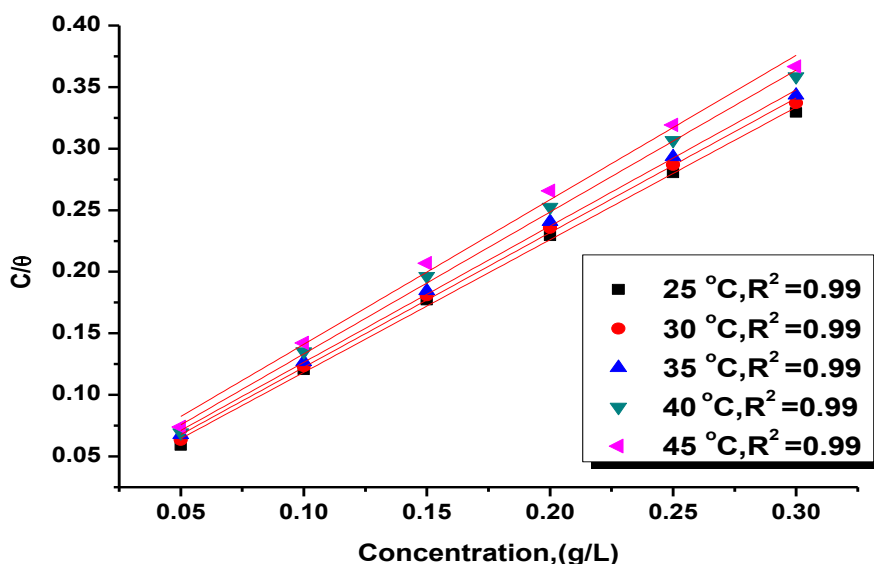


**Figure 7.** Langmuir diagrams for MS in presence of various concentrations of CDE at various temperatures (25-45°C)

The data of  $K_{ads}$  were lowered with the temperature rise indicating, that the interactions among the adsorbed CDE components and the surface of MS are decreasing and the CDE components come

to be simply transferable. Such values elucidate the lower in the IE with an improving temperature [28].

All the measured thermodynamic parameters are itemized in Table (5)  $\Delta H_{ads}$  have sign negative, signifying that the CDE adsorbed is an exothermic procedure, which incomes that the IE is minimum at maximum temperature, as a result of slow desorption of the inhibitor from the MS surface [29]. The  $\Delta S^{\circ}_{ads}$  of CDE on MS are negative sign and great. Table (6), which designates the lower of disorder due to the CDE or molecules adsorbed by removing of more molecules of water [30]. Negative sign ( $\Delta S^{\circ}_{ads}$ ) and ( $\Delta G^{\circ}_{ads}$ ) designates that the reaction was spontaneous and feasible. [31].

**Table 5.** Adsorption parameters of CDE on MS 1M HCl at various temperatures (25-45°C)

Temperature °C	$K_{ads} M^{-1}$	$-\Delta G^{\circ}_{ads} kJ mol^{-1}$	$-\Delta H^{\circ}_{ads} kJ mol^{-1}$	$-\Delta S^{\circ}_{ads} J mol^{-1}K^{-1}$	$R^2$
25	94	21.2	30	71.1	0.99
30	76	21		69.3	0.99
35	63	20.9		67.7	0.99
40	55	20.8		66.6	0.99
45	42	20.5		64.4	0.99

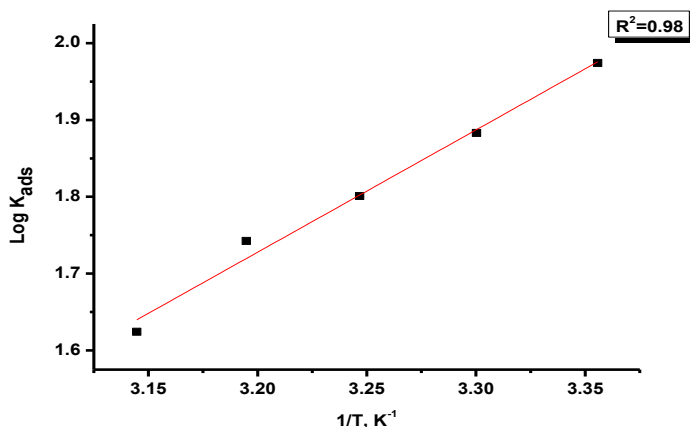


**Figure 8.** Log  $K_{ads}$  against  $1/T$  for CDE at different temperatures (25-45°C)

### 3.6 Kinetic-thermodynamic corrosion parameters

The influence of temperature and thermodynamic parameters in the MS corrosion presence and absence of various concentration CDE was achieved by the ML tests. These results have recorded in Table (6). The ( $E_a^*$ ), ( $\Delta H^*$ ) and ( $\Delta S^*$ ) for activation processes were measured using Arrhenius and transition state theory plots. The  $E_a^*$  of the MS in 1 M HCl was measured from the slope of the Arrhenius diagrams using equation 9, with and without the extract. A diagrams of  $\log k_{corr}$  against  $1/T$  with a slope =  $-E_a^*/2.303R$  given from ML tests in the absence and presence of the CDE provided a straight line Fig. (9) [32].

$$\text{Rate } (k_{\text{corr}}) = A \exp(-E_a^*/RT) \tag{9}$$

Where A is factor for Arrhenius pre-exponential, and  $k_{\text{corr}}$  is the rate of corrosion. This equation can be utilized to measure the  $E_a^*$  data of the corrosion rate reaction for sample in the absence and presence of the CDE. Table (6) demonstrates that  $E_a^*$  of the corrosion of MS in the presence of CDE is higher than in its absence. Improve in the  $E_a^*$  for MS dissolution in the presence of CDE may suggest a physical adsorption take place [33].

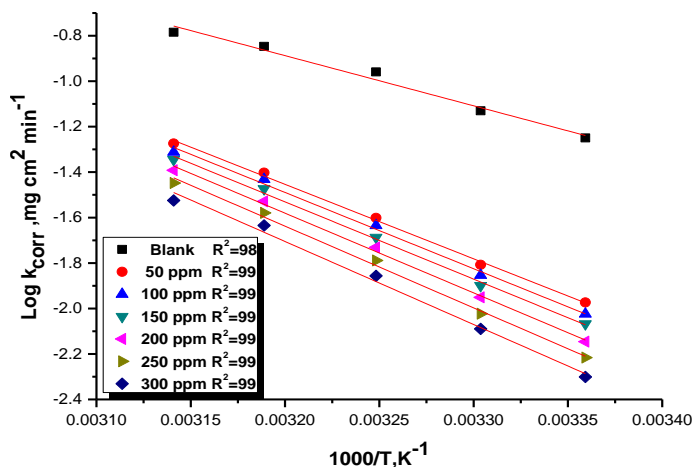


**Figure 9.** Arrhenius plots for MS after 120 minutes immersion in the absence and presence of different concentrations of CDE

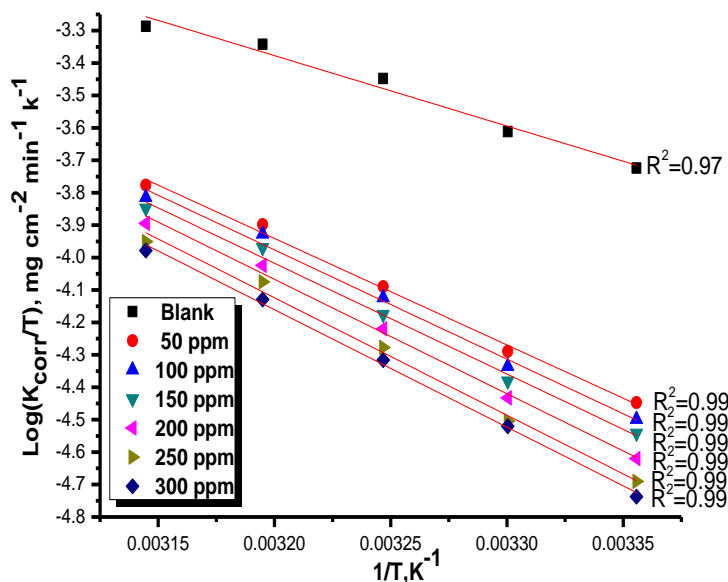


**Figure 10.** Log ( $k_{\text{corr}}/T$ ) vs. ( $1/T$ ) in the absence and presence of various concentrations of CDE

To calculate  $\Delta H^*$  and  $\Delta S^*$  with and without various concentrations of CDE with temperature rise [34], transition state theory can be used [35]:

$$\text{Rate } (k_{\text{corr}}) = RT/Nh \exp(\Delta S^*/R) \exp(-\Delta H^*/RT) \tag{10}$$

Where,  $h$  = constant Planck's. A diagrams of  $\log k_{\text{corr}}/T$  vs.  $1/T$  presented a straight line Fig (10) with a slope =  $-\Delta H^*/2.303 R$  and an intercept =  $\log R/Nh + \Delta S^*/2.303 R$ , from which the data of  $\Delta S^*$  and  $\Delta H^*$  were measured and registered in Table (6). The ( $\Delta H^*$ ) has positive sign indicate the endothermic manner of the process. This recommends that MS dissolution needs more energy in the presence of CDE. The positive sign of ( $\Delta S^*$ ) suggested that the activated complex in the rate determining stage shows dissociation rather than association [36].

**Table 6.** Parameters for activation of MS in the absence and presence of various concentrations of CDE

Conc. ppm	$E_a^*$ , kJ mol <sup>-1</sup>	$\Delta H^*$ , kJ mol <sup>-1</sup>	$-\Delta S^*$ , J mol <sup>-1</sup> K <sup>-1</sup>
1 M HCl	42.2	41.5	129.1
50	62.6	62.8	71.6
100	64.2	64.4	67.2
150	65.1	65.3	65.2
200	67.1	67.5	59.2
250	68.7	69.3	54.5
300	69.8	72.9	52.6

### 3.7 Fourier transforms infrared spectroscopy (FT-IR) analysis

It is well founded that FT-IR is a great method that can be utilized to recognize the kind of bonding predominantly functional group (s) presence in organic composite establish in Cleome Ddroserifolia. FT-IR test for MS surface can be beneficial for foreseeing whether an organic compound extract from Cleome Ddroserifolia are adsorbed or not. FT-IR were utilized to find the film formed from the extract components on the MS surface, this will isolate the MS surface from HCl solution [37].

FT-IR spectrum method based on analyzing the hindrance film designed on the MS surface. Figure (11) shows the FT-IR of the pure CDE. The – OH stretching frequency of the alcohol group seems at 3335 cm<sup>-1</sup> which has strong and broad intensity. The (C-H) stretching looks at (2928) cm<sup>-1</sup>. The C=C stretch seems at 1649 cm<sup>-1</sup>. The N=N stretching seems at 1397 cm<sup>-1</sup>. The (C-O) stretch seems at 1051 cm<sup>-1</sup>. The FT-IR of the film formed on the MS surface, after immersion in solution containing 1M HCl and 300 ppm of CDE, was represented in Figure (11b). The – OH stretching has moved from 3335 cm<sup>-1</sup> to 3330 cm<sup>-1</sup>. The (C-H) stretching has disappeared. The C=C stretch has moved from 1649 cm<sup>-1</sup> to 1635 cm<sup>-1</sup>. The N=N stretching has moved from 1397 cm<sup>-1</sup> to 1419 cm<sup>-1</sup>. The (C-O) stretch has moved from 1051 cm<sup>-1</sup> to 1002 cm<sup>-1</sup>. This remark indicates that CDE has coordinated with Fe<sup>2+</sup>, through the oxygen atom and nitrogen atom of the components exist in extract, and forming complex on the anodic sites on the MS surface [38].

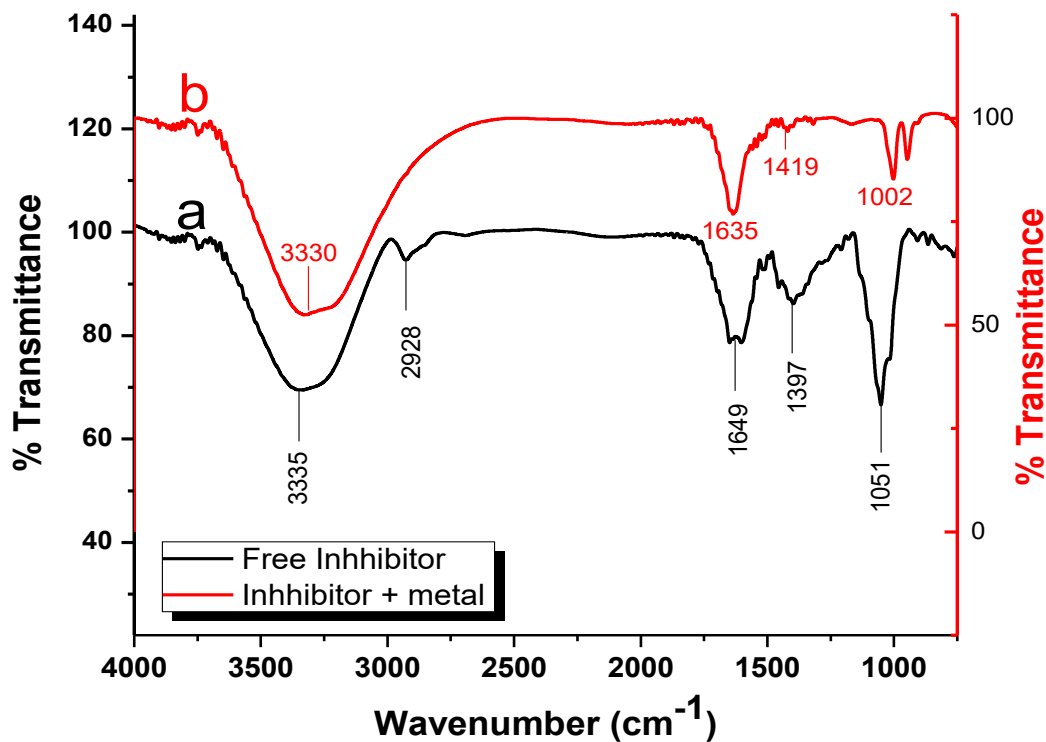


**Figure 11.** FT-IR spectroscopy of (a) CDE and (b) the film formed on the MS surface in 1M HCl + 300 ppm of CDE for 4 h at 25°C

### 3.8. Surface examination

#### 3.8.1 SEM test

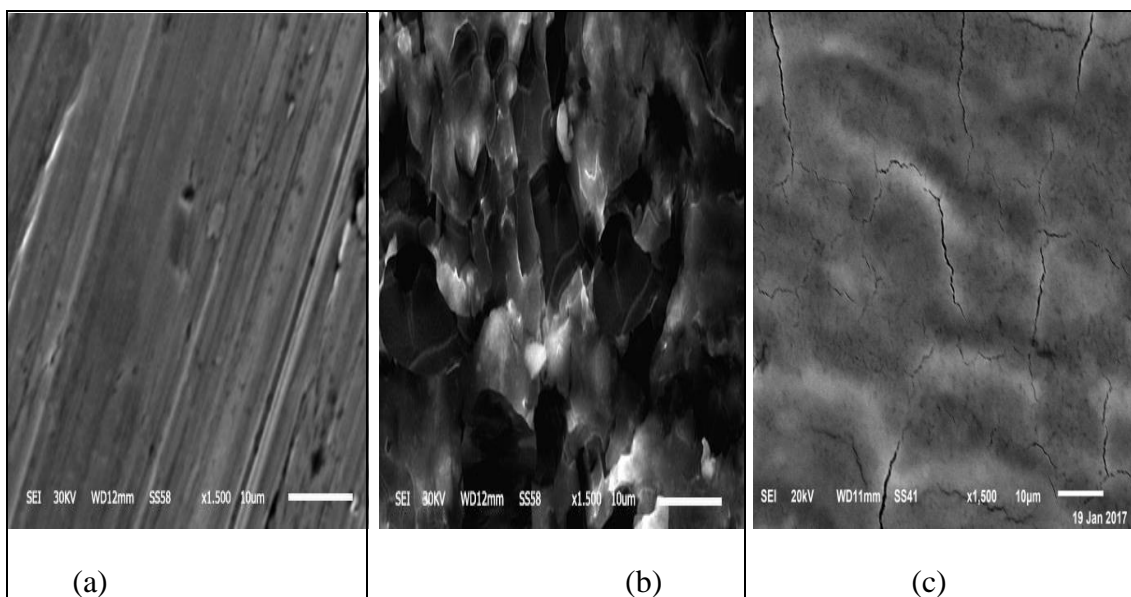
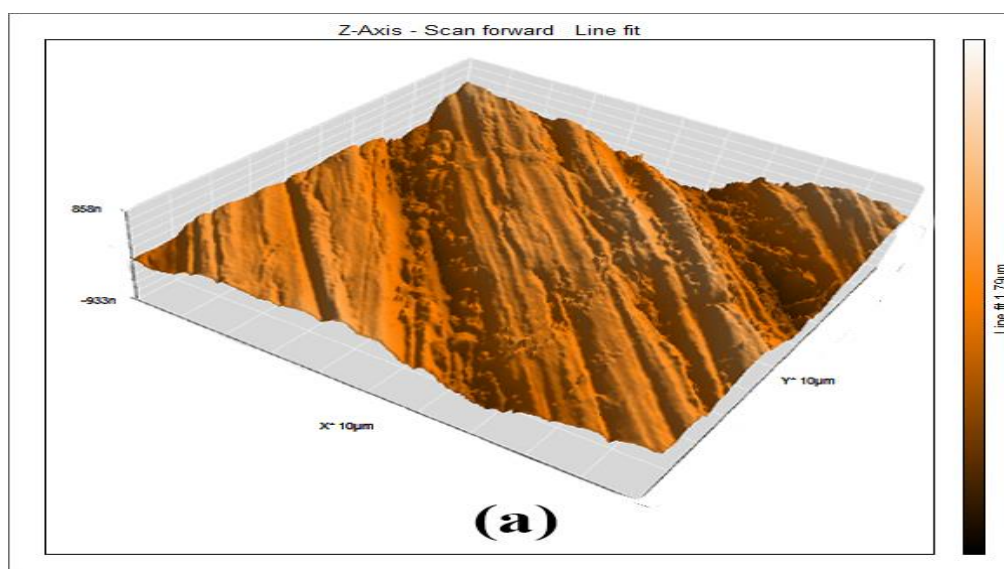


**Figure 12.** SEM picture of surface MS (a) before of immersion in 1M hydrochloric, (b) after 24 h of immersion in hydrochloric and (c) after 24 h of immersion in 1M hydrochloric + 300 ppm of CDE at 25.0°C

The effect of corrosion on the morphology of the MS surface was tested by recording the SEM images of the steel samples in 1M hydrochloric acid for 24 hours of immersion in the absence and presence of CDE. Fig. (12a) shows SEM images of polished MS with comparatively smooth surface, Fig. (12 b) displays SEM portrait of the surface of the research MS electrode after inundation in 1M hydrochloric solution for one day. The micrograph discloses that, the surface was powerfully damage. The rusty areas are exposed as black grooves in the coins with gray and white zones, which resemble to the dandruff of iron oxide. Fig. (13 c) demonstration SEM portrait for the surface of another MS coin after the inundation of the same time interval contains 300 ppm of CDE. The portrait exposes that, the hindrance MS surface is smoother than the corroded surface, an excellent shielding film presented on the MS. This approves the excellent hindrance efficiency of the inhibitor CDE.

### 3.8.2 AFM test

AFM is a great test for assembly of roughness statistics from a diversity of MS surfaces. AFM are coming recognized test of roughness examination [39]. As can be gotten from the AFM images, the surface is very pure for mirror MS coins with average roughness 33.43NM Fig. (13a) whereas, Fig. (13b, c) demonstrations the 3D images of the MS in lack (b) and attendance of 300 ppm CDE (c) In the absence of CDE, the surface of the MS is more corroded, with average roughness 667.5 nm Fig. (13b). By contrast, the average roughness was reduce to 91.724 nm in the presence of CDE at optimum concentration (300 ppm). From the results, we concluded that the lower in the roughness data is attributing to the creation of the hindrance layer of CDE on the MS surface.



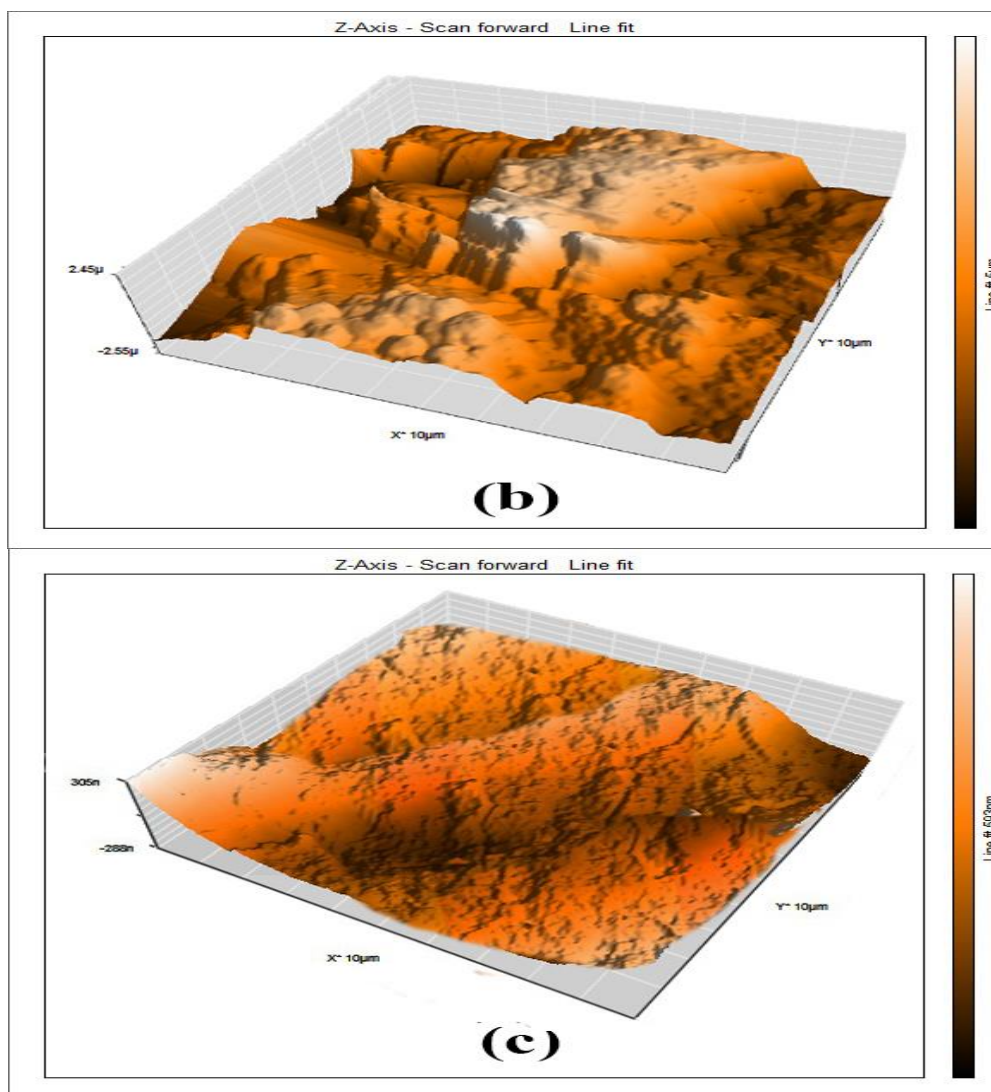


**Figure 13.** AFM portrait of MS surface (a) before of immersion in 1M hydrochloric, (b) after 24 h of immersion in 1M HCl and (c) after 24 h of immersion in hydrochloric + 300 ppm of CDE at 25°C

3.8.3. Comparison between Samwah extract and other mentioned before

Table 7 reviews some plant extracts used as corrosion inhibitors for MS in HCl solution, as we see the investigated Cleome Droserifolia (Samwah) extract is more efficient than those mentioned plant extracts in the table for MS in HCl solution and this is why we use this plant extracts as efficient one,

**Table 7.** Comparison of inhibition efficiencies of Cleome Droserifolia (Samwah) extract with other plant extracts in HCl solution

Inhibitor (Extract)	Sample	Medium	IE %	References
Cleome droserifolia (Samwah) extract	MS	HCl	>92	Our results
Aframomum melegueta leaf(800 mg/L)	MS	HCl	55.0	(40)

Phyllanthus amarus seed (4.0 g/l)	MS	HCl	80.1	(41)
date palm seed (2.5 g/l)	MS	HCl	86.8	(42)
Dacryodis edulis leaf (800 ml/L)	MS	HCl	70.0	(43)
reed leaves(800 mg/L)	MS	HCl	88.5	(44)
reed leaves(800 mg/l)	MS	HCl	88.1	(45)
green tea(500 ppm)	MS	HCl	82.0	(46)
fenugreek leaves(10% v/v)	MS	HCl	82.4	(47)
Datura stramonium leaf(20 ppm)	MS	HCl	88.1	(48)
Hibiscus sabdariffa leaf (50% (v/v)	MS	HCl	90.4	(49)
Mustardseed (4.0 g/l)	MS	HCl	62.2	(50)
lupine extract(0.65g/L)	MS	HCl	77.6	(51)

### 3.9. Mechanism of protection

The organic assembled adsorbed can be relate by two main kinds of relations: physical and chemisorption's adsorption [52]. Generally, two kinds of mechanisms of protection were planned. One was the creation of polymeric complexes with iron ions ( $\text{Fe}^{3+}$ ) depends on the practical conditions [53]. The other was the chemical adsorption of CDE constituents on iron surface [54]. The protective action of CDE does not occur by the simple blocking at the surface of iron, particularly at maximum temperature. It has been researched that with the rise in temperature, the disruptive effect of CDE components on iron surface improved. Some of the hydrophilic groups with positively charged atoms ( $\text{O}^+$ ) desorbed from the surface of iron and did more work to prevent the  $\text{H}^+$  from getting nearer to the MS surface. Consequently, CDE has hindrance both anodic and cathodic corrosion procedures at maximum temperatures.

## 4. CONCLUSIONS

Form the present study, it is concluded that:

The IE rises with the rise in the CDE concentrations and lower with improve in temperature. CDE components adsorbed on the MS surface following the Langmuir isotherm. TP diagram measurements indicate that CDE acted as a mixed kind inhibitor. FT-IR showed that the atoms present in the plant extract molecules form corrosion inhibiting layer by complexation with iron ions present on the MS surface. SEM and AFM images indicate the probability of creation of film on the surface of the MS. Based on the results of WL, TP, EIS and EFM measurements, the CDE is an effective inhibitor for MS in 1 M HCl.

## References

1. R. A. Prabhu, T. V. Venkatesha, A. V. Shanbhag, G. M. Kulkarni and R. G.Kalkhambkar, *Corros. Sci.*, 50(12) (2008)3356.
2. G. Mayakrishnan, S. Pitchai, K. Raman, A. R. Vincent and S. Nagarajan, *Ionics*, 17(9) (2011) 843.
3. A. Y. El-Etre, M. Abdallah and Z. E. El-Tantawy, *Corros. Sci.*, 47(2) (2005) 385.

4. M. Lashgari and A. M. Malek, *Electrochimica Acta*, 55(18) (2010) 5253.
5. F. Bentiss, M. Traisnel and M. Lagrenée, *Corros. Sci.*, 42(1) (2000) 127.
6. I. B. Obot, N. O. Obi-Egbedi, S. A. Umoren and E. E. Ebenso, *Int. J. Electrochem. Sci.*, 5(7) (2010) 994.
7. L. Herrag, B. Hammouti, S. Elkadiri, A. Aouniti, C. Jama, H. Vezin and F. Bentiss, *Corros. Sci.*, 52(9) (2010) 3042.
8. A. Ouchrif, M. Zegmout, B. Hammouti, A. Dafali, M. Benkaddour, A. Ramdani and S. Elkadiri, *Progress in organic coatings*, 53(4) (2005) 292.
9. S.M. Ezzat and A. A. Motaal, *Zeitschrift für Naturforschung C*, 67(5-6) (2012) 266.
10. K. M. Dawood, Y. M. Shabana, E. A. Fayzalla and E. A. El-Sherbiny, *J. Agric. Sci. Mans*; (2003) 5335.
11. M. A. Quraishi, A. Singh, V. K. Singh, D. K. Yadav and A. K. Singh, *Mater. Chem. Phys.*, 122(1) (2010) 114.
12. T. Ibrahim, E. Gomes, I. B. Obot, M. Khamis and M. Abou Zour, *J. Adhesion Sci. Technol.*, 30(23) (2016) 2523.
13. M. A. Amin, K. F. Khaled and S. A. Fadel-Allah, *Corros. Sci.*, 52(1) (2010) 140.
14. A. S. Fouda, A. M. El-Desoky and H. M. Hassan, *Int. J. Electrochem. Sci.*, 8 (2013) 5866.
15. I. B. Obot and N. O. Obi-Egbedi, *Corros. Sci.*, 52(1) (2010) 198.
16. A. Popova, E. Sokolova, S. Raicheva and M. Christov, *Corros. Sci.*, 45(1) (2003) 33.
17. A. Singh, I. Ahamad, V.K. Singh, M.A. Quraishi, *J. Solid State Electrochem*; 15(6) (2011) 1087.
18. E. S. Ferreira, C. Giacomelli, F. C. Giacomelli and A. Spinelli, *Mater. Chem. Phys.*, 83(1) (2004) 129.
19. W. H. Li, Q. He, S. T. Zhang, C. L. Pei and B. R. Hou, *J. Appl. Electrochem.*, 38(3) (2008) 289.
20. S. Zhang, Z. Tao, W. Li and B. Hou, *Appl. Surf. Sci.*, 255(15) (2009) 6757.
21. M. Outirite, M. Lagrenée, M. Lebrini, M. Traisnel, C. Jama, H. Vezin and F. Bentiss, *Electrochim. Acta*, 55(5) (2010) 1670.
22. G. E. Badr, *Corros. Sci.*, 51(11) (2009) 2529.
23. Z. Tao, S. Zhang, W. Li and B. Hou, *Corros. Sci.*, 51(11) (2009) 2588.
24. C. Verma, L. O. Olasunkanmi, E. E. Ebenso, M. A. Quraishi and I. B. Obot, *J. Phys. Chem. C*, 120(21) (2016) 1598.
25. B. M. Mistry and S. Jauhari, *Research on Chemical Intermediates*, 39(3) (2013) 1049.
26. J. Bessone, C. Mayer, K. Jüttner and W. J. Lorenz, *Electrochim. Acta*, 28(2) (1983) 171.
27. I. Epelboin, M. Keddam and H. Takenouti, *J. Appl. Electrochem.*, 2(1) (1972) 71.
28. X. Li, S. Deng, H. Fu, *Corros. Sci.*, 53(2011) 3241
29. B. M. Mistry and S. Jauhari, *Chemical Engineering Communications*, 201(7) (2014) 961.
30. P. Muthukrishnan, B. Jeyaprabha and P. Prakash, *Arabian J. Chem.*, 10 (2013) 2343.
31. K. P. Kumar, M. S. Pillai and G. R. Thusnavis, *Port. Electrochim. Acta*, 28(6) (2010) 373.
32. Li. Xianghong, S. Deng, and H. Fu, *Corros. Sci.*, 62 (2012) 163.
33. W. Li, Q. He, S. Zhang, C. Pei, B. Hou, *J. Appl. Electrochem.*, 38(2008) 289
34. M. Lebrini, F. Robert, A. Lecante and C. Roos, *Corros. Sci.*, 53(2) (2011) 687.
35. J. O. M. Bockris and A. K. N. Reddy *Modern electrochemistry*. Plenum, New York, 1977.
36. R.A. Prabhu, A.V. Shanbhag and T.V. Venkatesha, *J. Appl. Electrochem.*, 37(4) (2007) 491.
37. R. Vera, R. Schrebler, P. Cury, R. Del Rio and H. Romero, *J. Appl. Electrochem.*, 37(2007) 519
38. K. Nakamoto, New York: Wiley Interscience, 1986.
39. M. Hakeem, S. Rajendran and A. P. P. Regis, *J. Eng., Comput. Appl. Sci.*, 3(2) (2014) 1.
40. E.E. Oguzie, Z.O. Iheabunike, K.L. Oguzie, *J. Dispersion Sci. Technol.*, 34(2013) 516.
41. P.C. Okafor, M.E. Ikpi, I.E. Uwah, *Corros. Sci.*, 50 (2008) 2310.
42. S.A. Umoren, Z.M. Gasem, I.B. Obot, *Ind. Eng. Chem. Res.*, 52 (2013) 14855
43. E.E. Oguzie, C.K. Enenebeaku, C.O. Akalezi, *J. Colloid Interface Sci.*, 349 (2010) 283.
44. H. Cang, Z. Fei, H. Xiao, *Int. J. Electrochem. Sci.*, 7 (2012) 8869.

45. E.E. Oguzie. *Pigm.Resin Technol.*, 34 (2005)321.
46. A.Alsabagh, M.Migahed, M.Abdelraouf, *Int. J. Electrochem. Sci.*, 10 (2015)1855.
47. E.A.Noor, *Int. J. Electrochem. Sci.*, 2 (2007)996.
48. P.B.Raja, M.G.Sethuraman, *Surf. Rev. Lett.*, 14 (2007)1157.
49. E.E.Oguzie, *Port. Electrochim. Acta*, 26 (2008)303.
50. S.A.Umoren, *J. of Adhesion Science and Technology*, 30(17) (2016)1858.
51. A.M. Abdel-Gaber, B.A. Abd-El-Nabey, M. Saadawy, *Corros. Sci.*, 51 (2009)1038.
52. L. Narvaez, E. Cano and D. M. Bastidas, *J. Appl. Electrochem.*, 35(5) (2005) 499.
53. Li, Xianghong, Shuduan Deng, and Hui Fu, *Corros. Sci.*, 51(6) (2009)1344.
54. R. Saliyan and A. V. Adhikari, *Bull. Mater. Sci.*, 31(4) (2008).

© 2018 The Authors. Published by ESG ([www.electrochemsci.org](http://www.electrochemsci.org)). This article is an open access article distributed under the terms and conditions of the Creative Commons Attribution license (<http://creativecommons.org/licenses/by/4.0/>).